



OPEN ACCESS

EDITED BY

Shong Lau,
Salk Institute for Biological Studies,
United States

REVIEWED BY

Artur Llobet,
University of Barcelona, Spain
Joseph Zak,
University of Illinois at Chicago,
United States

*CORRESPONDENCE

Weitian Zhang
drzhangwt@163.com
Hui Wang
wangh2014@163.com
Haibo Shi
haibo99@hotmail.com

†These authors have contributed
equally to this work

SPECIALTY SECTION

This article was submitted to
Cellular Neuropathology,
a section of the journal
Frontiers in Cellular Neuroscience

RECEIVED 25 July 2022

ACCEPTED 05 October 2022

PUBLISHED 28 October 2022

CITATION

Li M, Liu Z, Lai K, Liu H, Gong L, Shi H,
Zhang W, Wang H and Shi H (2022)
Enhanced recruitment of glutamate
receptors underlies excitotoxicity
of mitral cells in acute
hyperammonemia.
Front. Cell. Neurosci. 16:1002671.
doi: 10.3389/fncel.2022.1002671

COPYRIGHT

© 2022 Li, Liu, Lai, Liu, Gong, Shi,
Zhang, Wang and Shi. This is an
open-access article distributed under
the terms of the [Creative Commons
Attribution License \(CC BY\)](https://creativecommons.org/licenses/by/4.0/). The use,
distribution or reproduction in other
forums is permitted, provided the
original author(s) and the copyright
owner(s) are credited and that the
original publication in this journal is
cited, in accordance with accepted
academic practice. No use, distribution
or reproduction is permitted which
does not comply with these terms.

Enhanced recruitment of glutamate receptors underlies excitotoxicity of mitral cells in acute hyperammonemia

Mingxian Li[†], Zhenqi Liu[†], Ke Lai[†], Hanwei Liu, Lina Gong,
Haosong Shi, Weitian Zhang*, Hui Wang* and Haibo Shi*

Department of Otorhinolaryngology, Shanghai Sixth People's Hospital Affiliated to Shanghai Jiao Tong University School of Medicine, Shanghai, China

Hepatic encephalopathy (HE)—a major complication of liver disease—has been found to increase the risk of olfactory dysfunction, which may be attributed to elevated levels of ammonia/ammonium in the blood and cerebrospinal fluid. However, the cellular mechanisms underlying hyperammonemia-induced olfactory dysfunction remain unclear. By performing patch-clamp recordings of mitral cells (MCs) in the mouse olfactory bulb (OB), we found that 3 mM ammonium (NH₄⁺) increased the spontaneous firing frequency and attenuated the amplitude, but synaptic blockers could prevent the changes, suggesting the important role of glutamate receptors in NH₄⁺-induced hyperexcitability of MCs. We also found NH₄⁺ reduced the currents of voltage-gated K⁺ channel (K_v), which may lead to the attenuation of spontaneous firing amplitude by NH₄⁺. Further studies demonstrated NH₄⁺ enhanced the amplitude and integral area of long-lasting spontaneous excitatory post-synaptic currents (sEPSCs) in acute OB slices. This enhancement of excitatory neurotransmission in MCs occurred independently of pre-synaptic glutamate release and re-uptake, and was prevented by the exocytosis inhibitor TAT-NSF700. In addition, an NH₄⁺-induced increase in expression of NR1 and GluR1 was detected on cytoplasmic membrane, indicating that increased trafficking of glutamate receptors on membrane surface in MCs is the core mechanism. Moreover, NH₄⁺-induced enhanced activity of glutamate receptors in acute OB slices caused cell death, which was prevented by antagonizing glutamate receptors or chelating intracellular calcium levels. Our study demonstrates that the enhancement of the activity and recruitment of glutamate receptor directly induces neuronal excitotoxicity, and contributes to the vulnerability of OB to acute hyperammonemia, thus providing a potential pathological mechanism of olfactory defects in patients with hyperammonemia and HE.

KEYWORDS

olfactory dysfunction, ammonium, mitral cell, glutamate receptor, excitotoxicity

Introduction

Overwhelming evidence indicates that olfactory dysfunction is associated with liver disease (Burch et al., 1978; Deems et al., 1993; Landis et al., 2004; Temmel et al., 2005; Zucco et al., 2006; Heiser et al., 2018), and 27–76% of patients with liver diseases experience olfactory defects, which can severely affect patient food cravings and intake (Deems et al., 1993; Temmel et al., 2005; Heiser et al., 2018). Hepatic encephalopathy (HE) is a major complication of liver dysfunction, and poor olfactory function has been associated with severe cases. Even patients with minimal HE present with compromised thresholds of odor identification (Temmel et al., 2005; Zucco et al., 2006; Heiser et al., 2018). Ammonium (NH_4^+)—a proposed major determinants of HE—is toxic and can lead to functional disturbances in the central nervous system by altering neuronal excitability and synaptic transmission (Back et al., 2011; Oja et al., 2017; Jayakumar and Norenberg, 2018).

Ammonium exerts different neuronal effects in different brain regions. It influences the neuronal physiological properties through increasing intracellular calcium levels and altering cytoplasmic pH (Lazarenko et al., 2017). More importantly, NH_4^+ can affect glutamatergic and gamma-aminobutyric acid (GABA) neurotransmission and disturb intracellular signal transduction pathways (i.e., the glutamate-NO-cGMP pathway), resulting in impairment of neuronal plasticity, learning ability, memory, or even death in acute and chronic hyperammonemia (Sanchez-Perez and Felipo, 2006; Cabrera-Pastor et al., 2016; Lazarenko et al., 2017; Sancho-Alonso et al., 2022). In the CA1 region of rat hippocampus, acute NH_4^+ administration inhibits neuronal long-term potentiation through GABA-enhancing neurosteroids (Izumi et al., 2013). In the chronic hyperammonemia rat, decreased NR2A and NR2B subunit expressions in the hippocampus lead to impaired learning and memory (Yonden et al., 2010). Acute hyperammonemia in mice can impair cortical inhibitory network and trigger seizures by depolarizing neuronal GABA reversal potential (Rangroo Thrane et al., 2013). In rats with chronic hyperammonemia, the amount of GABA transporter GAT-3 is elevated, resulting in the increased extracellular accumulation of GABA leading to motor in-coordination (Cabrera-Pastor et al., 2018). Mitral cells (MCs), are the projecting neurons in the OB and responsible for olfactory encoding and transmission (Wang et al., 2003; Padmanabhan and Urban, 2010; Boyd et al., 2012; Nagayama et al., 2014). Its apical dendrites ramify in the glomerulus, where they receive glutamatergic inputs from the nerves of olfactory sensory neurons (OSNs) and external tufted cells (ETCs). And MCs also receive inhibitory inputs from the interneurons including periglomerular cells (PG) and granule cells (GCs) through dendrodendritic synapses. Despite compelling evidence of the effects of NH_4^+ on neurotransmission and neuronal excitability, its pathological mechanism in the olfactory system has never been explored.

In this study, we investigated whether NH_4^+ alters the excitability of MCs and explored the potential cellular mechanism of MC excitotoxicity by NH_4^+ . Our results demonstrated that 3 mM NH_4^+ increases the spontaneous firing rates and attenuates the amplitude by potentiating glutamate receptor activity and suppressing Kv currents, leading to MC hyperexcitability. Furthermore, not only have we found that NH_4^+ elevates the amplitude and integral area of spontaneous excitatory post-synaptic currents (sEPSCs), but also NH_4^+ administration leads to excitotoxicity and cell death through enhancing the activity and membrane trafficking of glutamate receptors, independently of the alteration in glutamate re-uptake and pre-synaptic glutamate release, suggesting elevated activity and expression of glutamate receptors by NH_4^+ underlie increased MC excitability and excitotoxicity in the OB.

Materials and methods

Ethical approval

All animal procedures were performed in accordance with the guiding principles of the National Institutes of Health Guide for the Care and Use of Laboratory Animals and were approved by the Ethics Committee of the Shanghai Sixth People's Hospital affiliated to Shanghai Jiao Tong University School of Medicine. All efforts were made to avoid causing unnecessary pain and suffering as possible.

Slice preparation and solutions

C57BL/6J mice (aged 15–20 days) were anesthetized with isoflurane before decapitation, as previously described (Chen et al., 2016). The brain was excised and immersed in ice-cold oxygenated artificial cerebrospinal fluid (aCSF) containing (in mM): 124 NaCl, 5 KCl, 1.2 KH_2PO_4 , 2.4 CaCl_2 , 1 MgCl_2 , 24 NaHCO_3 , and 10 glucose, saturated with 95% O_2 and 5% CO_2 . The forebrain containing the OB was dissected and sectioned into transverse 300 μm -thick slices using a vibratome (VT-1200s, Leica, Nussloch, Germany). The slices were incubated in aCSF with 95% O_2 and 5% CO_2 at 37°C for 40 min to recover cell viability and then maintained at room temperature (23–25°C) before patch-clamp recordings.

Reagents

All chemicals and drugs were purchased from Sigma-Aldrich (St. Louis, MO, USA), unless otherwise indicated. The common reagents used in the experiment were NH_4Cl , bicuculline (Bic), strychnine (Stry), DL-2-amino-5-phosphonopentanoic acid (APV) and 1,2,3,4-tetrahydro-6-nitro-2,3-dioxo-benzo[f]quinoxaline-7-sulfonamide disodium

salt hydrate (NBQX). We prepared different concentrations (1, 3, 5 and 10 mM) of NH_4Cl solution with an equimolar mass substitute of NaCl. The pH of NH_4Cl solution in aCSF saturated with 95% O_2 and 5% CO_2 was consistent with that of pure aCSF. DL-*threo*- β -benzyloxyaspartic acid (TBOA) and dynasore were purchased from Tocris (Bristol, United Kingdom). TAT-NSF700 was obtained from Anaspec (Fremont, CA, USA). Bic, Stry, APV, NBQX, TBOA, BAPTA-AM, TAT-NSF700, and dynasore were prepared in stock solution at -20°C and later diluted to a final concentration in aCSF before use. The final concentrations of Bic, Stry, APV, NBQX, TBOA, dynasore, TAT-NSF700, and BAPTA-AM were 10, 3, 50, 20, 30, 40, 5, and 40 μM , respectively. During physiological recordings, MCs were exposed to different reagents through a square-tube gravity perfusion system at a speed of 1 mL/min, continuously gassed with 95% O_2 and 5% CO_2 . All experiments were performed at room temperature.

Mitral cell identification

The MCs in the OB slices were identified by their location, size, shape, and primary dendrites of their cell bodies. MC cell bodies were located in the MC layer, had a diameter of $>20 \mu\text{m}$, and their soma structures were characterized by different shapes (triangles, polygons, or ovoids). The soma was readily identified using a CCD camera with a $60\times$ water immersion objective attached to an upright microscope (Examiner.A1, ZEISS, Gottingen, Germany).

Cell-attached recordings

Patch pipettes (resistance of 3–5 $\text{M}\Omega$) for the soma recordings were fabricated from borosilicate capillary glass (World Precision Instruments, Sarasota, FL, USA) using a vertical pipette puller (PC-10; Narishige, Tokyo, Japan). To record the physiological activity of MCs without causing perturbation of the intracellular homeostasis, spontaneous action potentials were recorded using a loose-patch cell-attached configuration in the current-clamp mode without any current injection. The pipette was only then filled with aCSF. Data were acquired using a MultiClamp 700B (Axon, 5 kHz low-pass-filtered; 1550, sampled at 50 kHz) and pClamp6 software. The gain of the amplifier was set to the highest possible range below saturation to increase the signal to noise ratio and improve data quality.

Whole-cell voltage-clamp recordings

To investigate the effects of NH_4^+ on the excitatory synaptic receptors of MC, we performed voltage-clamp recordings in a whole-cell configuration. The pipette solution used in all whole-cell recordings contained (in mM): 130 K-gluconate, 5 KCl, 0.6

ethylene glycol-bis(β -aminoethyl)-N,N,N',N'-tetraacetic acid (EGTA), 10 4-(2-hydroxyethyl)-1-piperazineethane sulfonic acid (HEPES), 4 MgCl_2 , 3 Na_2ATP and 0.3 Na_3GTP and 10 sodium creatine phosphate dibasic tetrahydrate (adjusted to pH 7.3 with KOH). The bath offset potential and electrode capacitance were compensated for before sealing the cell membrane. The series resistance varied from 5 to 15 $\text{M}\Omega$ among cells and was adjusted by 75–90% to maintain $<15 \text{M}\Omega$ throughout the recordings. Cells showing changes in series resistance of $>15\%$ during recording were omitted from the analysis. We recorded the spontaneous post-synaptic currents (sPSCs) that displayed long-lasting depolarization and continued to record spontaneous excitatory PSCs (sEPSCs) in the presence of Bic and Stry at a holding potential of -60mV . Bic and Stry were used to suppress inhibitory currents mediated by GABA and glycine. sEPSCs were recorded in the control (Bic + Stry), drug solutions, and wash solution.

To examine the effect of NH_4^+ on excitatory inputs from OSNs to MCs, we placed a bipolar stimulation electrode at the OSN nerve stubs in a subset of experiments to stimulate afferent inputs to the recorded cell. Recordings were made 200–400 μm from the stimulation electrode. The threshold for evoked responses, defined as the stimulation threshold, was measured by gradually increasing the intensity until evoked EPSCs (eEPSCs) or burst firings were triggered. The average stimulation threshold was $2.55 \pm 0.23 \text{V}$. The eEPSC represents as “all or none” response (Gire and Schoppa, 2009). To evoke a stable eEPSC, we used a high intensity of stimulation. Single-pulse stimulations were performed with an interval of 20 s over a recording period of 100 s. Paired-pulse stimulation was conducted with an inter-pulse time interval of 2,000 ms, since evoked EPSCs (eEPSCs) displayed a long refractory period and needed more time to recover to baseline. The stimulations were repeated 10 times with an inter-trial interval of 15 s in the control, drug solutions, and wash solution. We further analyzed the paired-pulse ratio (PPR: P2/P1) to represent changes in pre-synaptic release probability.

Furthermore, raw voltage-gated sodium (Nav) and Kv currents were recorded in voltage-clamp mode at a holding potential of -70mV and were activated by step depolarization from -70 to 40 mV in 10 mV increments, by using test pulses 500 ms in duration.

Whole-cell current-clamp recordings

We also recorded the spontaneous action potentials at I_0 in whole-cell current-clamp mode in the aCSF, and drug solutions. Resting membrane potential (RMP) was measured as well. To measure the membrane resistance (R_m), the evoked depolarized membrane potential was recorded through injecting a current of 10 pA at the holding potential of -60mV . The rise time constant (τ) was measured by Clampfit 10.6 software. R_m

was calculated using the equation: $\tau = R_m C_m$, where C_m is membrane capacitance.

Membrane surface protein immunoblotting

The fresh mouse OB tissues were incubated in aCSF and 3 mM NH_4Cl respectively for 1 h and then washed with cold PBS (1 \times) and lysed in mild protein lysis buffer (Regent A in cell membrane protein extraction kit, Beyotime, Biotechnology, Shanghai, China) and supplemented with protease inhibitor (1 \times) (phenylmethanesulfonyl fluoride, Beyotime). This was followed by grinding using a glass homogenizer for 80 times, and subsequent centrifugation at $700 \times g$ for 10 min. The suspension was collected and centrifuged at $14,000 \times g$ for 30 min. As a result, the membrane proteins were pelleted at the bottom of the centrifuge tube. After discarding the supernatant, we added 200 μl Regent B and centrifuged the solution at $14,000 \times g$ for 5 min, and collected the membrane protein solution. The solution was boiled in 1 \times SDS sample buffer for 5 min and used for western blot. The samples were centrifuged and supernatant protein was separated on 7.5% sodium dodecyl sulfate-polyacrylamide gel electrophoresis (SDS-PAGE) Gel (Invitrogen, Carlsbad, CA, USA). Separated proteins were transferred onto a NC membrane, blocked in 5% non-fat dry milk for at least 1 h at room temperature and subsequently incubated overnight at 4°C on a shaker with primary antibody against rabbit anti-NR1, rabbit anti-GluR1 (purchased from abclonal, Wuhan, China, 1:1000 dilution) and rabbit anti-Na/K-ATPase (Servicebio, Wuhan, China, 1:1000 dilution). After incubation with primary antibodies, the membranes were incubated with goat anti-rabbit horseradish peroxidase conjugated secondary antibodies (abclonal, 1:5000 dilution) for 1 h at room temperature. Na/K-ATPase was chosen as the loading control. Western blots were performed for at least three times and the densitometry analysis was conducted using Image-J Software.

Assessment of cell vitality with calcein-AM/PI co-staining

To assess the levels of NH_4^+ -induced neurotoxicity in MCs, we sectioned OB slices to a thickness of 220 μm with a vibratome (Leica) and pre-treated the slices with control, NH_4Cl , APV + NBQX, APV + NBQX + NH_4Cl , TAT-NSF700, TAT-NSF700 + NH_4Cl , BAPTA-AM, or BAPTA-AM + NH_4Cl solution for 1 h before incubation with 1 μM calcein-AM and 2 μM propidium iodide (PI) (Solarbio, Beijing, China) for 15 min at 37°C. Following three washes with aCSF, the slices were fixed with 4% paraformaldehyde for 1 h and mounted, with a coverslip. Slices were observed by confocal microscopy

(LSM-710, ZEISS, Thornwood, NY, USA), and live cells and apoptotic nuclei were counted at 40 \times magnification. To evaluate the vitality of projecting neurons, we acquired the regions of interest, including the external plexiform and MC layers. The number of stained cells was measured using Image-J software (National Institutes of Health, Bethesda, MD, USA).

Statistical analysis

The amplitude, integral area, and frequency of sEPSCs were used to quantify synaptic events. All electrophysiological data were analyzed by Clampfit 10.2 software (Molecular Devices, San Jose, CA, USA). The parameter of minimum allowed duration in the threshold search was 0.001 or 300 ms to detect the peaks of spontaneous firing or EPSCs, respectively. Peaks were detected automatically, but each event was visually inspected to prevent the inclusion of stochastic artifacts. To quantify the features of spontaneous firing, we fitted the inter-event interval of each recording using a Gaussian function. The 3-min duration of the control period was used for quantitative evaluation after the electrophysiological activity of the cells reached stability. All drug treatments lasted for 10 min, and the time window used for analysis was 5 min, after confirming drug activity. The washout time was 6 min, and the last 3-min recording was used for analysis. The average eEPSC amplitude, integral area, and duration under control conditions were normalized to 1.0 for visual presentation and reported as absolute values in the text. Data were analyzed using SPSS 26.0 software (IBM SPSS, Chicago, IL, USA) and are presented as mean \pm standard error of the mean (SEM). GraphPad Prism 9 (GraphPad Software, San Diego, CA, USA) and Adobe Illustrator CC (Adobe Systems, San Jose, CA, USA) were used to generate graphics. Three-group comparisons were evaluated using one-way analysis of variance (ANOVA) with a *post hoc* least significant difference (LSD) test to determine intergroup differences. A paired or unpaired Student's *t*-test was used for two-group comparisons. Statistical significance was set at $p < 0.05$.

Results

Mitral cells exhibited typical spontaneous burst firings and long-lasting excitatory depolarized currents

Mitral cells, as one of the major neurons projecting to the piriform cortex, receive excitatory inputs from OSNs and ETCs, and inhibitory regulation from interneurons, including PG and GCs (Figure 1A). We first explored the

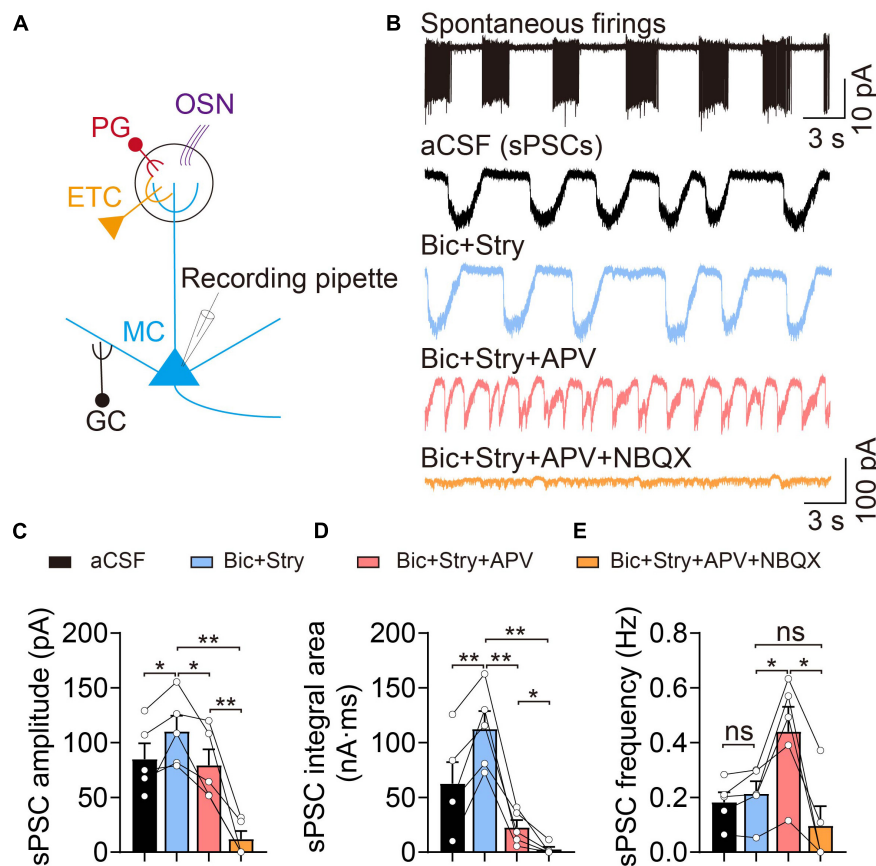


FIGURE 1

Electrophysiological properties of mitral cells (MCs). (A) Basic representation of MC morphology and electrophysiological recording using the patch-clamp technique; olfactory sensory neuron (OSN, purple), external tufted cell (ETC, yellow), periglomerular cell (PG, red), and granule cell (GC, black). (B) Cell-attached recording of spontaneous burst firings (upper) and corresponding whole-cell recordings of spontaneous post-synaptic currents (sPSCs) in aCSF, Bic + Stry, Bic + Stry + APV, and Bic + Stry + APV + NBQX in the same MC. (C–E) sPSC amplitude, integral area, and frequency in aCSF, Bic + Stry, Bic + Stry + APV, and Bic + Stry + APV + NBQX. Elevated sPSC amplitude and integral area in the presence of Bic + Stry and inhibition of sPSC by APV and NBQX revealed that the excitatory inputs in MC are regulated by glutamate receptors involving NMDA and AMPA receptors. Error bars represent standard error; * $p < 0.05$, ** $p < 0.01$; ns, not significant; one-way ANOVA with LSD *post-hoc* test.

electrophysiological properties of MCs in cell-attached voltage-clamp configurations. Previous studies have shown that MCs exert spontaneously active and heterogeneous firing patterns that encode olfactory cues. In our study, most MCs displayed spontaneous and rhythmic burst firing patterns, however other firing characteristics were also present, such as regular and irregular firing (Figure 1B). Interestingly, when the cell membrane was broken through in the voltage-clamp mode at a holding potential of -60 mV, they always appeared waved and long-lasting depolarized currents, defined as sPSCs (also LLD) (Figure 1B). Previous studies have shown the sPSCs consist of both *N*-methyl-*D*-aspartate (NMDA) and non-NMDA receptor components, and the non-NMDA receptor regulates the initiation of sPSCs (Carlson et al., 2000). The sPSCs are generated by a multistep, diffuse mechanism in the distal portion of the apical dendrite (Schoppa and Westbrook, 2001; Gire et al., 2012). The sPSC amplitude

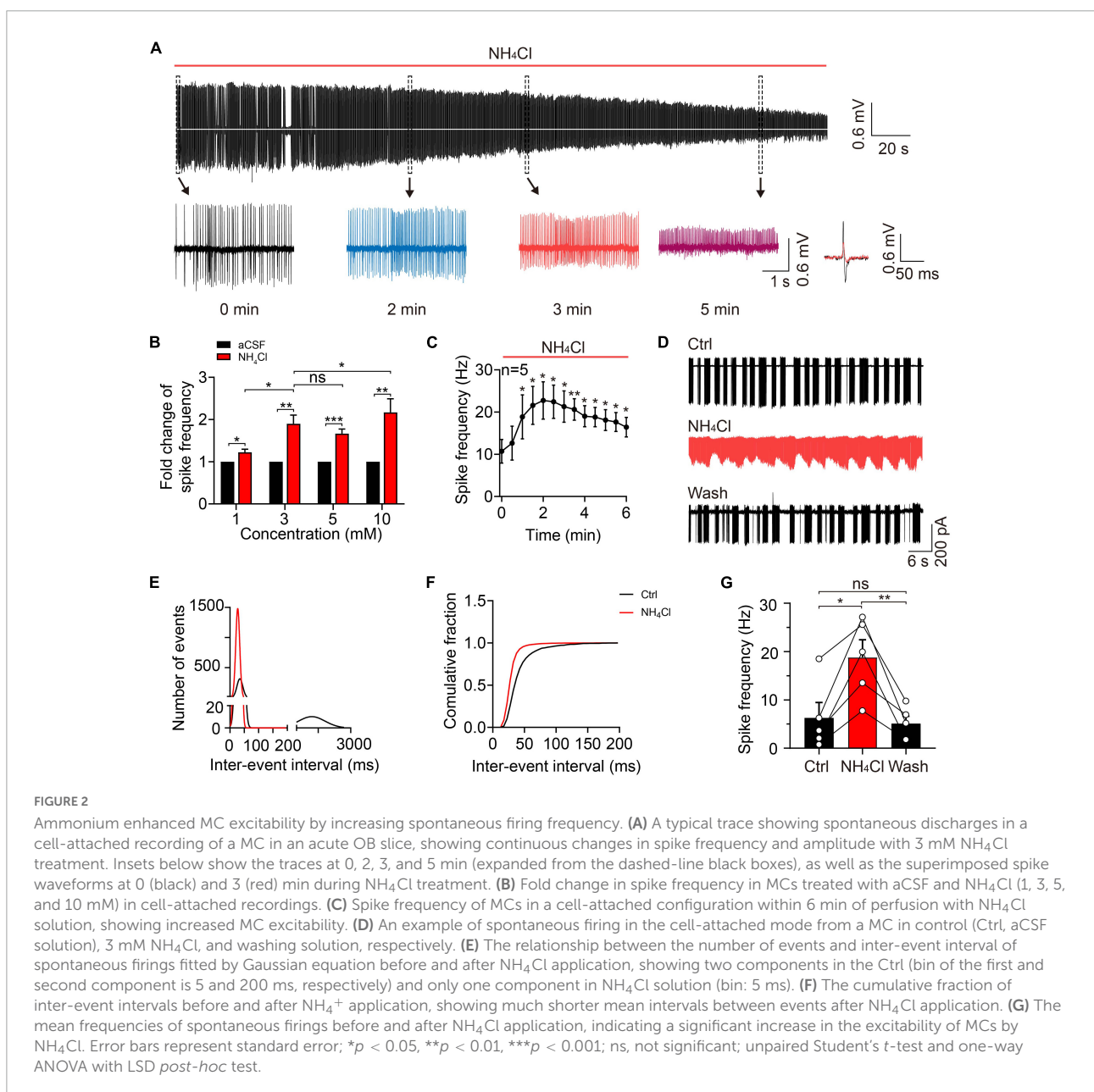
(control: 84.97 ± 14.37 pA, Bic + Stry: 110.20 ± 14.32 pA, $n = 5$, $p = 0.042$) and integral area (control: 62.45 ± 19.66 nA·ms, Bic + Stry: 112.40 ± 16.48 nA·ms, $n = 5$, $p = 0.008$) were altered by inhibiting GABA_A and glycine receptors, while the sPSC frequency remained unchanged in this study ($n = 5$, $p = 0.150$, Figures 1C,D). After applying a cocktail of excitatory and inhibitory synaptic blockers, sEPSC amplitude (Bic + Stry + APV: 79.31 ± 14.54 pA, Bic + Stry + APV + NBQX: 11.96 ± 7.35 pA, $n = 5$), integral area (Bic + Stry + APV: 22.42 ± 6.87 nA·ms, Bic + Stry + APV + NBQX: 2.55 ± 2.45 nA·ms, $n = 5$), and frequency (Bic + Stry + APV: 0.44 ± 0.09 Hz, Bic + Stry + APV + NBQX: 0.10 ± 0.07 Hz, $n = 5$) were drastically reduced (all $p < 0.05$, Figures 1B–E). Interestingly, the frequency of sEPSCs was significantly increased before and after antagonizing NMDA receptor (Bic + Stry: 0.21 ± 0.04 Hz, Bic + Stry + APV: 0.44 ± 0.09 Hz, $n = 5$, $p = 0.022$). Consistent

with previous studies, our results demonstrate that MCs are mainly characterized by spontaneous rhythmic burst firing and long-lasting depolarized currents, which are mainly regulated by glutamate receptors involving NMDA and α -amino-3-hydroxy-5-methyl-4-isoxazole propionate (AMPA) receptors.

Ammonium enhanced mitral cell excitatory activity by accelerating spontaneous firing rates

To explore the acute effect of NH_4^+ on MC spontaneous firings, we continuously recorded spontaneous action potentials

for 10 min with a cell-attached configuration. To determine the appropriate concentration of NH_4Cl solution in the study, we perfused 1, 3, 5, and 10 mM NH_4Cl in the OB slices and observed its role in MCs spontaneous firings. We found that 3, 5, and 10 mM NH_4Cl increased the frequency of spontaneous firings by 89.88% ($n = 5$, $p = 0.003$), 66.42% ($n = 7$, $p < 0.001$), and 116.75% ($n = 7$, $p = 0.004$) over the initial 3-min period, which then weakened as the NH_4Cl application continued, and the amplitude of the depolarized and hyperpolarized action potential tended to decrease and even disappear (Figures 2A,B). In addition, application of 1 mM NH_4Cl also increased the spike frequency by 22.39% ($n = 5$, $p = 0.015$) but did not change the amplitude of action potentials.



We also observed that high concentrations (e.g., 5 and 10 mM) of NH_4Cl induced an increment regarding spontaneous firing rates was not much higher than 3 mM NH_4Cl . Moreover, the percentage of cells with disappearing spikes, were positively associated with the increasing concentrations of NH_4Cl (0/5 cells in 1 mM NH_4Cl , 5/10 cells in 3 mM NH_4Cl , 4/7 cells in 5 mM NH_4Cl , and 7/7 cells in 10 mM NH_4Cl). However, these concentrations of NH_4Cl mentioned above, are higher than the concentration of NH_4Cl in patients with HE ($311 \pm 67 \mu\text{mol/L}$), and 3 mM NH_4Cl was an appropriate concentration to explore its acute neuronal excitotoxicity (Ong et al., 2003; Montes-Cortes et al., 2020). Moreover, we found the NH_4^+ -induced frequency alteration occurred in a time-dependent manner: At first, the frequency was accelerated to approximately three times that of the control and then decreased to a relatively stable frequency with persistent NH_4Cl application over 6 min at which the frequency was still higher than that in aCSF ($n = 5$, $p < 0.001$) (Figure 2C). Furthermore, to identify whether 3 mM NH_4Cl could induce a same phenomenon by using HEPES-dialyzed pipette solution, we recorded the spike frequency and RMP in whole-cell current-clamp mode, finding the change of spike frequency is same with cell-attached recordings and a depolarized trend of RMP with a significant transient depolarization within 4-min NH_4Cl (Supplementary Figure 1).

To clarify the effect of NH_4^+ on MC spike activity and whether the NH_4^+ -induced effect could be reversed, we recorded spontaneous firing in control (aCSF) buffer for 5 min, NH_4Cl solution for 10 min, and washing solution for 12 min. To analyze the spike frequency, we measured the inter-event interval of 3-min events in the control and NH_4Cl groups and plotted the data as binned and cumulative frequency histograms (Figures 2D–F). MCs with typical burst firing (in the control) had two components in the fitted curve, the first component representing the inter-event interval of intra-burst firings and the second component showing the inter-burst interval (first component 34.53 ± 10.14 ms, 5-ms bins, second component $1,210 \pm 610$ ms, 200-ms bins; $n = 5$); following the NH_4Cl treatment, the curve not only shifted toward zero but transformed into a single component (28.14 ± 6.94 ms, 5-ms bins; $n = 5$; Figure 2E), indicating elevated spike frequency. The left shift of the cumulative curve after NH_4Cl application indicated a reduction in the mean inter-event interval (Figure 2F). The NH_4^+ -induced excitation of MCs could be partially reversed by washing solution, but it took ~ 10 min for the spike frequency to return to baseline (control: 6.26 ± 3.19 Hz, NH_4Cl : 18.80 ± 3.65 Hz, Wash: 5.09 ± 1.54 Hz, $n = 5$, $p = 0.011$; Figure 2G). These results demonstrate that NH_4^+ can facilitate MC excitation by increasing spontaneous firing frequency, but the mechanisms behind the NH_4^+ -induced reduction in spike amplitude remain to be explored.

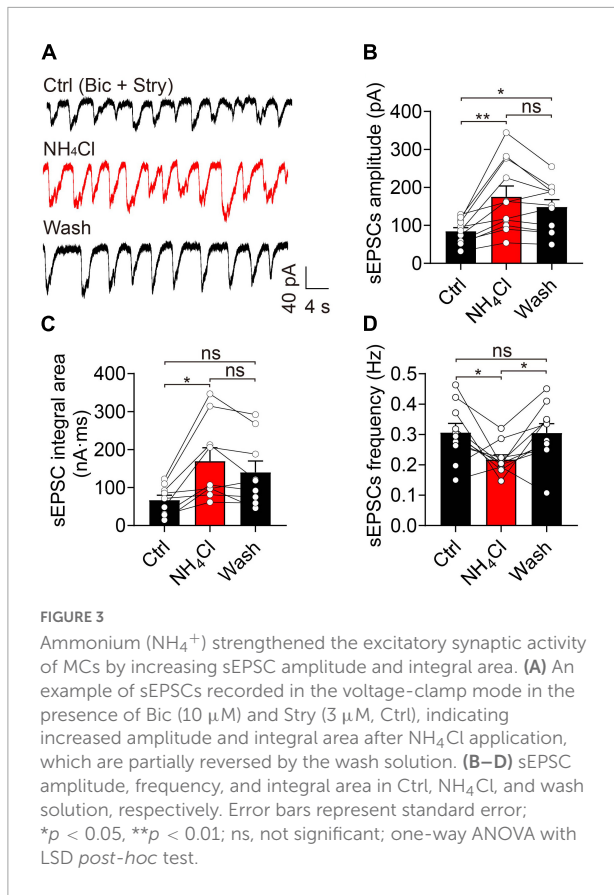
To explore the potential mechanism of NH_4^+ -induced effects on the frequency and amplitude of spontaneous firings, we conducted the electrophysiological recordings in the

presence of APV + NBQX + Bic + Stry. In the experiment, the results showed that NH_4^+ temporarily decreased the amplitudes of inward (I_{inward}) and outward (I_{outward}) currents of spontaneous action potentials and increased the spike frequency within 4-min of NH_4Cl perfusion which may be due to the depolarized membrane potential initially, but the amplitudes of I_{inward} and I_{outward} and the spike frequency gradually reversed to the baseline (in aCSF) 4-min after which was not consistent with those in the absence of post-synaptic receptors blockers (Supplementary Figures 2A–F). We further detected the effect of NH_4^+ on the raw currents of Nav (I_{Na}) and Kv (I_{K}) channels, showing that the amplitude of I_{Na} was decreased, and the number of I_{Na} events at -40 mV were increased by 4-min NH_4Cl perfusion, and the changes were recovered at 8-min, while the amplitude of I_{K} were attenuated with 4- and 8-min treatment (Supplementary Figures 3A–D). Interestingly, we also found that the gradual depolarization of RMP by NH_4^+ matched with the increased frequency and decreased amplitude of spontaneous firings, indicating NH_4^+ -induced changes of spontaneous firings may be attributed to the depolarized membrane potential (Supplementary Figures 2G,H). In the experiment, the membrane resistance remained unchanged during NH_4Cl application (Ctrl: 194.80 ± 18.92 M Ω , NH_4^+ : 195.30 ± 14.74 M Ω , $n = 5$, $p = 0.904$) (Supplementary Figures 2I,J). In summary, we consider NH_4^+ -induced changes of spike frequency and amplitude are caused by depolarized membrane potential, but the membrane potential is depolarized transiently when blocking excitatory and inhibitory synaptic inputs, which indicates that overactivity of glutamate receptors but not inhibitory receptors might be the potential factor to aggravate membrane depolarization and evoke MC excitotoxicity because the reversal potential of chloride ion is close to the RMP in the study.

Ammonium increased the amplitude and integral area of spontaneous excitatory post-synaptic currents

Elevated levels of NH_4^+ in the brain can increase glutamine synthesis, which can be catalyzed by glutaminase and decomposed to glutamate. NH_4^+ exerts neurotoxicity by facilitating NMDA receptor activation and activating the Ca^{2+} -NO-cGMP signaling pathway (Cauli et al., 2009). Spontaneous burst firing was mainly regulated by glutamate receptors in the OB and NH_4^+ -induced increment of spike frequency could be prevented by synaptic blockers (Hayar et al., 2004; Nagayama et al., 2014). Therefore, we hypothesized that the activity of glutamate receptors was upregulated by NH_4^+ resulting in depolarized membrane potential and increased spontaneous MC firing.

NH_4Cl increased the amplitude of sEPSCs to 168% that of the control, which was partially reversed by washing for



6 min (control: 84.54 ± 9.59 pA, NH_4Cl : 175.40 ± 28.28 pA, wash: 148.60 ± 19.11 pA, $n = 11$, $p = 0.012$; **Figures 3A,B**). NH_4Cl had a similar effect on sEPSC integral area (control: 66.86 ± 12.82 nA·ms, NH_4Cl : 169.40 ± 35.23 nA·ms, wash: 139.90 ± 29.95 nA·ms, $n = 9$, $p = 0.042$; **Figure 3C**). In contrast, the sEPSC frequency was reduced from 0.31 ± 0.03 Hz to 0.22 ± 0.02 Hz by NH_4Cl treatment, and could be reversed to 0.30 ± 0.03 Hz by washing ($n = 10$, $p = 0.037$; **Figure 3D**). These results indicate that NH_4^+ promotes MC neuronal excitability by increasing the amplitude and integral area of sEPSCs.

Ammonium boosted mitral cell synaptic activity independently of glutamate release from pre-synaptic terminals

To determine the potential mechanism of the NH_4^+ -induced increase of amplitude and integral area of sEPSCs, we recorded eEPSCs by stimulating the olfactory sensory nerves and examined whether NH_4^+ could facilitate glutamate release from pre-synaptic terminals. In this experiment, NH_4^+ substantially decreased the amplitude of eEPSCs to 46% that of the control during single-pulse stimuli with 20-s intervals

(control: 202.20 ± 66.21 pA, NH_4Cl : 93.61 ± 33.51 pA, wash: 287.30 ± 105.70 pA, $n = 4$, $p = 0.003$; **Figures 4A–C**), with no change observed in the integral area of eEPSCs ($n = 4$, $p = 0.250$). Washing recovered the amplitude of eEPSCs to an even greater extent than that of the control group (**Figure 4B**). To test whether the NH_4^+ -induced reduction in pre-synaptic glutamate release was due to changes in pre-synaptic release probability, we analyzed the PPR (P2/P1). We found that the amplitudes of both the first and second eEPSCs were markedly attenuated by NH_4Cl ($35.79 \pm 3.08\%$ that of the control in first EPSCs, $n = 7$, $p = 0.039$; $36.04 \pm 6.47\%$ that of the control in second EPSCs, $n = 5$, $p < 0.001$), while the mean PPR was unchanged ($n = 5$, $p = 0.826$; **Figures 4D–G**). These results suggest that NH_4^+ suppresses glutamate release from pre-synaptic terminals without influencing the release probability, which does not explain the enhanced activity of sEPSCs induced by NH_4^+ . Although we attempted to record miniature EPSCs (mEPSCs) and further confirm the above results, mEPSCs were particularly weak when perfusing 1 μM TTX.

Blocking glutamate re-uptake did not influence the ammonium-induced increase in excitatory synaptic activity

Ammonium can inhibit excitatory amino acid transporters (EAATs), which is likely one of the major factors influencing synaptic activity and neuronal excitation in a hyperammonemia model (**Butterworth, 1993**). Accordingly, we used TBOA to block EAATs in the OB and examined whether NH_4^+ could prevent intercellular glutamate re-uptake and, in so doing, promote overactivity of glutamate receptors. We recorded sEPSCs during the sequential application of control, NH_4Cl , and $\text{NH}_4\text{Cl} + \text{TBOA}$ solutions (**Figure 5A**). The TBOA + NH_4Cl treatment increased the amplitude (control: 96.70 ± 8.64 pA, NH_4Cl : 196.90 ± 25.10 pA, $\text{NH}_4\text{Cl} + \text{TBOA}$: 365.70 ± 42.72 pA, $n = 11$, $p < 0.001$) and integral area (control: 53.75 ± 10.78 nA·ms, NH_4Cl : 142.30 ± 32.52 nA·ms, $\text{NH}_4\text{Cl} + \text{TBOA}$: $1,067.00 \pm 238.10$ nA·ms, $n = 11$, $p < 0.001$) by 85.73 and 649.82% that of the NH_4Cl only group, respectively (**Figures 5B,C**). In contrast, the sEPSCs frequency was reduced by TBOA (control: 0.33 ± 0.02 Hz, NH_4Cl : 0.20 ± 0.02 Hz, $\text{NH}_4\text{Cl} + \text{TBOA}$: 0.10 ± 0.01 Hz, $n = 11$, $p < 0.001$; **Figure 5D**). Moreover, we first blocked EAATs and then applied NH_4Cl and found that the mean values of amplitude (control: 116.20 ± 14.41 pA, TBOA: 270.90 ± 45.06 pA, TBOA + NH_4Cl : 331.50 ± 42.41 pA, $n = 5$, $p = 0.004$) and integral area (control: 67.09 ± 17.37 nA·ms, TBOA: 420.50 ± 153.70 nA·ms, TBOA + NH_4Cl : 830.80 ± 325.60 nA·ms, $n = 5$, $p = 0.069$) of sEPSCs were also markedly increased by NH_4^+ though there were no significant statistical difference of integral area and frequency between only TBOA and TBOA + NH_4Cl with one way ANOVA analysis (**Figures 5E–H**). These results revealed

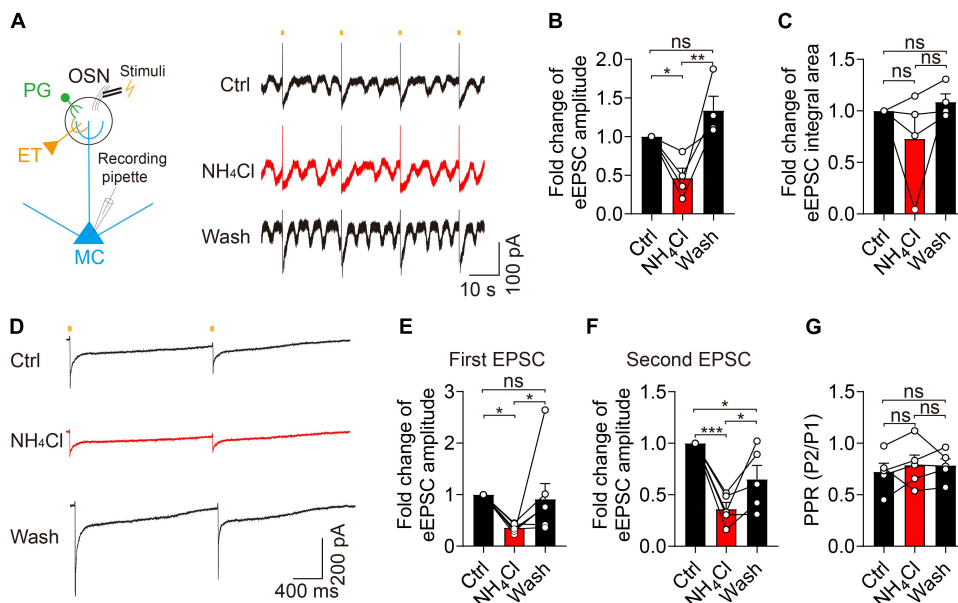


FIGURE 4

Ammonium (NH_4^+) reduced the pre-synaptic glutamate release in MCs without affecting pre-synaptic release probability. **(A)** Left panel showing MC recording of evoked EPSCs (eEPSCs) after stimulating OSN stubs with a bipolar electrode. Right panel showing eEPSCs from a MC by continuous single-pulse stimuli with 20 s intervals in Ctrl, NH_4Cl , and wash solution, respectively, in the presence of Bic + Stry. **(B–C)** Fold change of eEPSC amplitude, and integral area in Ctrl, NH_4Cl , and wash solution, respectively. **(D)** An example of eEPSCs recorded from a MC in Ctrl, NH_4Cl , and wash solution, respectively. EPSCs were evoked by paired-pulse stimuli with an interval of 2,000 ms (determined by the slow recovery course of eEPSCs). **(E–G)** Pooled data showing fold changes of the first and second eEPSC amplitude and PPR (paired-pulse ratio, P2/P1) in Ctrl, NH_4Cl , and wash solution, respectively. Error bars represent standard error; * $p < 0.05$, ** $p < 0.01$, *** $p < 0.001$; ns, not significant; one-way ANOVA with LSD *post-hoc* test.

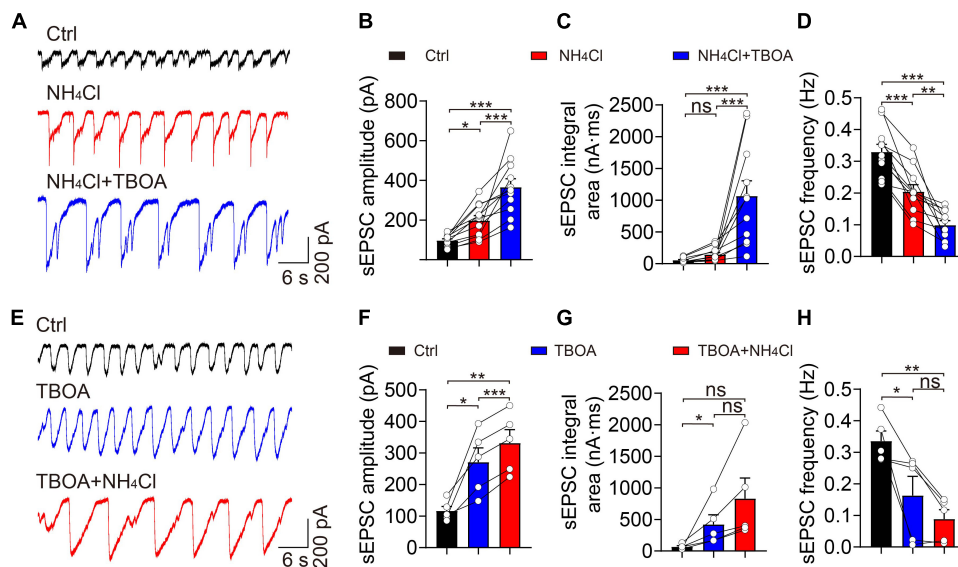


FIGURE 5

Blockade of EAATs did not attenuate NH_4^+ -induced potentiation of excitatory synaptic activity. **(A)** Representative traces showing sEPSCs recorded in a voltage-clamp configuration in the presence of Bic + Stry, showing the changes in sEPSC amplitude and integral area in Ctrl, NH_4Cl , and NH_4Cl + TBOA (30 μM), respectively. **(B–D)** sEPSC amplitude, integral area, and frequency in sequential treatments with Ctrl, NH_4Cl , and NH_4Cl + TBOA. **(E)** Typical sEPSC traces from a MC in sequential treatments of Ctrl, TBOA, and TBOA + NH_4Cl . **(F–H)** *Post hoc* analysis of sEPSC amplitude, integral area, and frequency in Ctrl, TBOA, and TBOA + NH_4Cl , respectively. Error bars represent standard error; * $p < 0.05$, ** $p < 0.01$, *** $p < 0.001$; ns, not significant; one-way ANOVA with LSD *post-hoc* test.

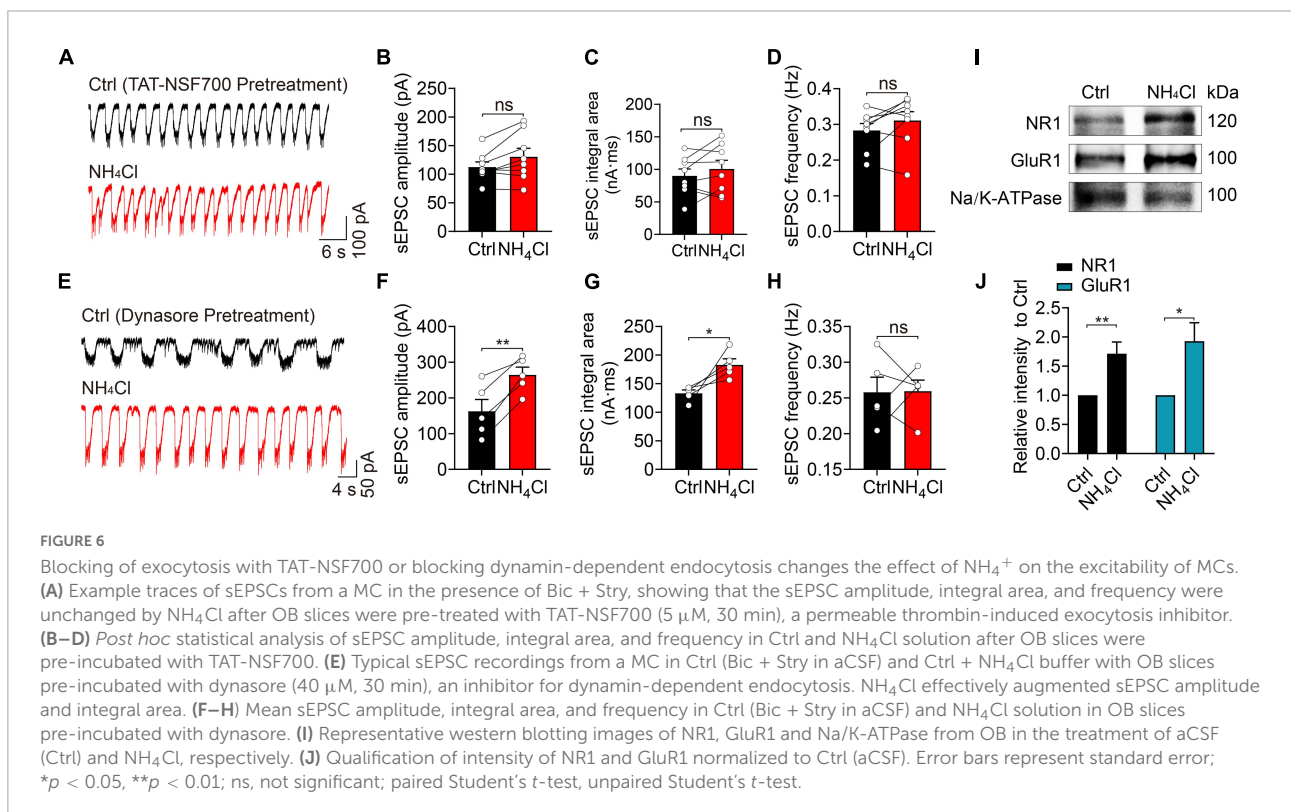
that the activity of EAATs in the OB was not inhibited by NH_4^+ and that sEPSCs could still be enhanced by NH_4^+ when blocking EAATs. In other words, the enhanced excitatory post-synaptic events induced by NH_4^+ in MCs was not attributed to the suppression of glutamate uptake.

Ammonium enhanced the trafficking of glutamate receptors to the cytoplasmic membrane

We hypothesized that NH_4^+ might increase the expression of glutamate receptors to potentiate excitatory synaptic transmission in MCs. We employed TAT-NSF700, an *N*-ethylmaleimide-sensitive factor (NSF) inhibitor fusion polypeptide that can permeate the cell membrane and interact with intracellular organelles, preventing vesicles from transporting intracellular proteins to the cytoplasmic membrane (Calvert et al., 2007). Pre-treatment of the OB slices with TAT-NSF700 for 30 min effectively alleviated the spontaneous excitatory synaptic activity induced by NH_4^+ (Figure 6A); NH_4^+ did not change the amplitude, integral area, or frequency of sEPSCs (amplitude: $n = 8$, $p = 0.052$; integral area: $n = 8$, $p = 0.225$; frequency: $n = 8$, $p = 0.163$; Figures 6B–D). This suggests that NH_4^+ increased the active recruitment of glutamate receptors from the cytosolic pool to the membrane.

Alternatively, slowed endocytosis of membrane glutamate receptors may also increase sEPSC activity. To explore this, we pre-incubated OB slices with 40 μM dynasore—a dynamin inhibitor that can block the internalization of membrane proteins—and found that NH_4^+ still increased the amplitude (control: 162.80 ± 32.85 pA, NH_4Cl : 264.40 ± 21.91 pA, $n = 5$, $p = 0.004$) and integral area (control: 133.10 ± 5.90 nA·ms, NH_4Cl : 182.90 ± 10.46 nA·ms, $n = 5$, $p = 0.033$) of sEPSCs by 62.41 and 37.42% that of the control group, respectively (Figures 6E–G). The frequency of sEPSCs was not affected by NH_4^+ ($n = 5$, $p = 0.955$) (Figure 6H). Interestingly, blocking the endocytosis of glutamate receptors with dynasore pre-treatment effectively increased NH_4^+ -induced excitatory synaptic activity (amplitude: NH_4^+ : 175.4 ± 28.28 pA, NH_4Cl with dynasore: 264.40 ± 21.91 pA, $p < 0.001$; integral area: NH_4Cl : 169.40 ± 35.23 nA·ms, NH_4Cl with dynasore: 182.90 ± 10.46 nA·ms, $p = 0.039$). These results demonstrate that when endocytosis is blocked, NH_4^+ can promote the accumulation of glutamate receptors on cell membrane as well as the recruitment of intracellular pool to the cell membrane, thereby synergistically enhancing excitability.

To directly demonstrate whether NH_4^+ can increase the recruitment of glutamate receptors to cell membrane surface, we carried out western blotting analysis of glutamate receptor subunits on cell membrane fractions after OB slices were treated with NH_4Cl solution. Considering that NR1 and GluR1 are the basic subunits of NMDA and AMPA receptor, respectively, we



tested the expression of NR1 and GluR1, with Na/K-ATPase as the internal reference. The immunoblotting analysis revealed that NH_4^+ significantly elevated the level of NR1 and GluR1 without affecting Na/K-ATPase expression on cytoplasmic membrane (NR1: elevated 1.71 ± 0.20 -fold in NH_4^+ , $n = 5$, $p = 0.007$; GluR1: elevated 1.93 ± 0.32 -fold in NH_4^+ , $n = 4$, $p = 0.027$) (Figures 6I,J). These results further demonstrated that NH_4^+ elevates the expression of glutamate receptors, resulting in enhanced MC excitability through promoting the recruitment of glutamate receptors to cytoplasmic membrane.

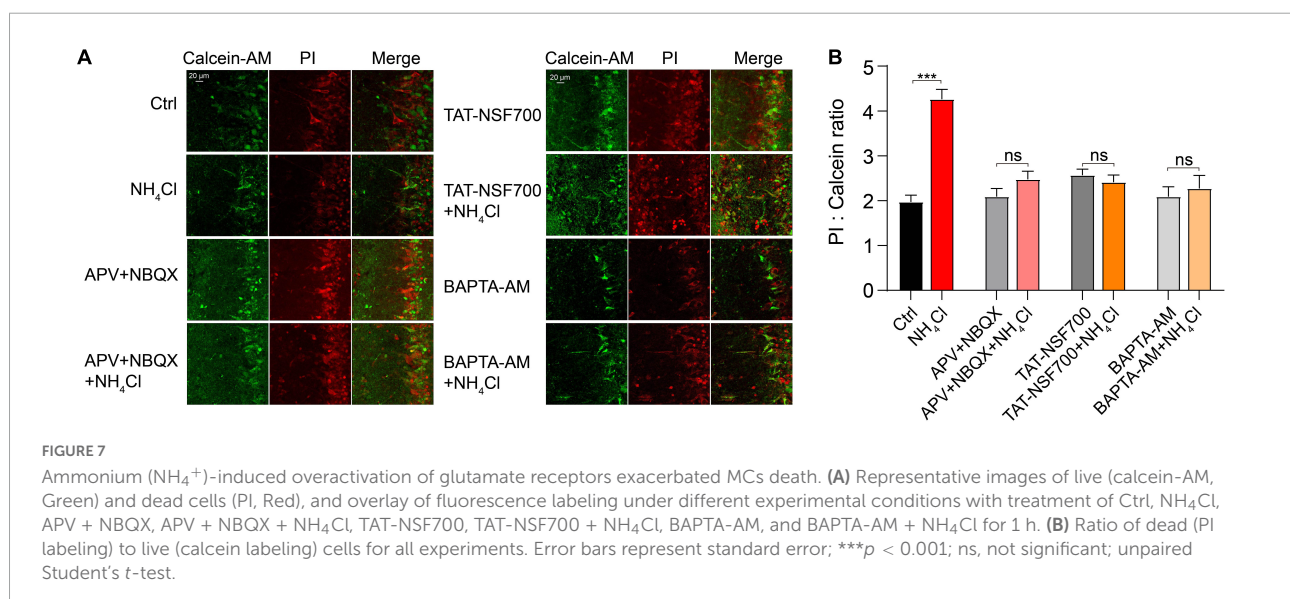
Upregulation of glutamate receptors induced by ammonium exacerbated cell death

To assess the effect of the upregulated membrane expression of glutamate receptors on cell viability, we assessed the neurotoxicity induced by NH_4^+ using a cell death assay. OB slices were pre-treated with control and NH_4^+ for 1 h, and then calcein-AM/PI co-staining was applied to quantify the ratio of dead/live cells. NH_4^+ increased the dead/live ratio from 1.97 ± 0.16 to 4.26 ± 0.22 that of the control (nine images from three slices, $p < 0.001$), while APV + NBQX, TAT-NSF700, and BAPTA-AM effectively attenuated NH_4^+ -induced cell death (NH_4Cl : 4.26 ± 0.22 , APV + NBQX + NH_4Cl : 2.47 ± 0.18 , TAT-NSF700 + NH_4Cl : 2.41 ± 0.16 , BAPTA-AM + NH_4Cl : 2.27 ± 0.29 , $p < 0.001$; Figures 7A,B). Interestingly, BAPTA-AM pre-treatment remarkably mitigated the NH_4^+ -induced cell death (NH_4Cl : 4.26 ± 0.22 , BAPTA-AM + NH_4Cl : 2.27 ± 0.29 , $p < 0.001$, Figures 7A,B). These results indicate that NH_4^+ can aggravate cell death, and buffering calcium can suppress the NH_4^+ -induced neurotoxicity.

Discussion

Growing evidence demonstrates that patients with liver diseases, especially those with HE, develop a poor olfactory ability to detect and identify odors (Temmel et al., 2005; Zucco et al., 2006). In these patients, serious liver dysfunction can lead to cognitive and motor impairment, coma, and death owing to the accumulation of many metabolic byproducts, among which NH_4^+ is a key contributor to cerebral dysfunction (Jayakumar and Norenberg, 2018). The present study provides evidence for NH_4^+ -induced excitotoxicity of MCs through the enhanced activity of glutamate receptors, revealing the potential mechanism of olfactory impairment in patients with HE.

In the olfactory system, MCs are characterized by burst firing patterns in complex neuronal circuits with neighboring cells (Nagayama et al., 2014). MC has a primary dendrite that forms a highly branched tufts within a single glomerulus, where these tufts receive a multistep signaling input forming glomerulus-specific slow and synchronized bursts or LLD (Gire et al., 2012). These signals include glutamatergic inputs from OSN axons and ETC dendrites, glutamate spillover and lateral excitation between MC-MC/MC-TC dendrodendritic connections, metabolic glutamate receptors, and electrical coupling between dendrites (Nicoll and Jahr, 1982; Isaacson and Strowbridge, 1998; Margrie et al., 2001; De Saint Jan et al., 2009; Gire and Schoppa, 2009; Moran et al., 2021). The initiation of a LLD driven by a glomerulus-specific network, is mainly mediated by AMPA receptors, and NMDA receptors modulate the amplitude and duration of the LLD (Carlson et al., 2000). Our observation that blocking the NMDA receptors results in an increased frequency, which may be attributed to the fast activation and desensitization kinetics of AMPA receptors (Figure 1B).



Interestingly, we also found that 3 mM NH_4Cl induced significant changes of spontaneous firings in MCs, showing increased frequency and decreased amplitude of spontaneous firings, whereas the increased frequency and decreased amplitude demonstrated to be transient and then recovered after blocking excitatory and inhibitory synaptic inputs. This phenomenon indicates that the enhanced activity of glutamate receptors by NH_4^+ plays an essential role in the continuous decrease of spike amplitude, as evidenced by the fact that activation of glutamate receptors in MCs can evoke a long-lasting membrane depolarization (Carlson et al., 2000). Furthermore, Nav and Kv channels are critical for spike initiation, propagation, and firing patterns in central neurons (Catterall et al., 2005; Bean, 2007). Lazarenko et al. has shown NH_4^+ depolarized neuronal membrane potential, probably by influencing Na^+ -sensitive background sodium leak channel NALCN (Lu et al., 2007; Lazarenko et al., 2017). NH_4Cl has been found to be one of the agonists of acid-sensitive ion channels, and may activate the channels contributing to the formation of the transient depolarization of membrane potential (Pidoplichko and Dani, 2006). In our study, transient membrane depolarization and the concurrent suppression of Nav and Kv currents by NH_4^+ , jointly lead to the amplitude attenuation during the initial NH_4^+ application. In addition, previous studies have shown NH_4^+ induced the decreased K^+ conductance and the elevation of extracellular K^+ which led to membrane depolarization (Allert et al., 1998; Rangroo Thrane et al., 2013). Except for the effect of glutamate receptors, the sustaining attenuation of Kv currents by NH_4^+ may be a necessary factor to depolarize membrane potential, resulting in progressive attenuation of amplitude in spontaneous firings.

In our study, we found that acute hyperammonemia can elevate the amplitude and integral area of sEPSCs in MCs, leading to neuronal hyperexcitability and neurotoxicity in OB slices, but the potential mechanism remains to be discussed. At first, olfactory sensory nerves in the superficial OB form monosynaptic connection to the apical dendrite tufts of MCs and the ETCs action potentials mediate the feedforward excitation of MCs in the specific glomerulus (Chen et al., 1997; Hayar et al., 2004; De Saint Jan et al., 2009). In our study, suprathreshold intensity stimulation of OSN stubs did not increase the eEPSC activity in the treatment of NH_4Cl , indicating the OSN-MC and OSN-ETC-MC synaptic transmission did not play an essential role in NH_4^+ -induced enhancement of sEPSCs. On the contrary, the pre-synaptic glutamate release was inhibited, consistently with the results of a previous study (Szerb and Butterworth, 1992). Second, it has been shown that ammonia facilitates the synthesis of glutamate and increase the accumulation of extracellular glutamate, which might boost the glutamate spillover and lateral excitation between MC-MC/MC-TC dendrodendritic synapses in the

glomeruli (Nicoll and Jahr, 1982; Aroniadou-Anderjaska et al., 1999; Cauli et al., 2009; Cabrera-Pastor et al., 2019). We excluded this possibility because the amplitude and integral area of sEPSCs were still enlarged by NH_4^+ after we blocked the uptake of glutamate with TBOA. Third, previous studies have revealed NH_4^+ plays a crucial role in triggering neuronal overexcitability by altering glutamate receptor expression in the central nervous system in acute and chronic hyperammonemia (Kosenkov et al., 2018; Sancho-Alonso et al., 2022). However, different results have been reported for glutamate receptor expression in the hippocampus and cerebellum of hyperammonemia rats. Some studies found that chronic hyperammonemia can elevate the membrane expression of NMDA receptors, and alter the expression of AMPA receptor subunits in the hippocampus (Cabrera-Pastor et al., 2016; Hernandez-Rabaza et al., 2016; Kosenkov et al., 2018). However, others found that ammonia reduces MK801 binding to NMDA receptors and the surface expression of the NR1 and NR2A subunits in ammonia-treated cerebellar neurons (Rao et al., 1991; Sanchez-Perez and Felipo, 2006). The C1 domain of NR1 has three serine residues (890, 896, and 897), whose phosphorylation has been implicated in modulating NMDA receptor trafficking and clustering (Llansola et al., 2005). The ammonia-induced increase in phosphorylation of these three serine residues is associated with the expression of NMDA receptors, but the potential mechanism is unclear. In our study, we demonstrated that NH_4^+ can dynamically regulate the recycling and trafficking of glutamate receptors and increase their expressions on the membrane in MCs. This process might be due to NH_4^+ -activated Ca^{2+} -dependent post-translational modifications of glutamate receptors on the membrane and/or the recruitment of a pre-existing pool of glutamate receptors.

We acknowledge some limitations to our study. For example, we did not identify the effect of NH_4^+ on the neurotransmission of MCs in a glutamate receptor-knockout mouse model. Our study was performed using *in vitro* acute OB slices, which revealed the cellular mechanism of NH_4^+ toxicity in the olfactory system; however, it did not consider pathological activity or the influence of NH_4^+ on olfactory function in an *in vivo* model.

In conclusion, we investigated the potential mechanisms underlying MC excitotoxicity in an *in vitro* model of acute hyperammonemia. We found that NH_4^+ increases spontaneous firing frequency and decreases the amplitude through the joint effects of enhanced glutamate receptor activity and reduced Kv currents. The results also demonstrated enhanced glutamate receptor activity by increasing the recruitment of glutamate receptors on the MC cytoplasmic membrane, contributing to cell overexcitability and neurotoxicity. This study implicates a potential pathological mechanism of olfactory defects in patients with hyperammonemia and HE, and glutamate receptors and their trafficking as potential molecular and

cellular targets for protection and intervention against NH_4^+ -induced neurotoxicity.

Data availability statement

The original contributions presented in the study are included in the article/**Supplementary material**, further inquiries can be directed to the corresponding authors.

Ethics statement

The animal study was reviewed and approved by Ethics Committee of the Shanghai Sixth People's Hospital Affiliated to Shanghai Jiao Tong University School of Medicine.

Author contributions

ML, ZL, and KL: experiments and data collection. HBS, HW, and WZ: data analysis and manuscript writing. WZ, HW, HBS, ZL, KL, HL, LG, HSS, and ML: experiment design and manuscript writing. All authors have reviewed the manuscript.

Funding

This work was sponsored by the International Cooperation and Exchange of the National Natural Science Foundation of China (82020108008) and the National Natural Science Foundation of China (82000993/82171140).

Acknowledgments

We would like to thank Editage (www.editage.cn) for English language editing.

Conflict of interest

The authors declare that the research was conducted in the absence of any commercial or financial relationships that could be construed as a potential conflict of interest.

Publisher's note

All claims expressed in this article are solely those of the authors and do not necessarily represent those of their affiliated organizations, or those of the publisher, the editors and the reviewers. Any product that may be evaluated in this article, or claim that may be made by its manufacturer, is not guaranteed or endorsed by the publisher.

Supplementary material

The Supplementary Material for this article can be found online at: <https://www.frontiersin.org/articles/10.3389/fncel.2022.1002671/full#supplementary-material>

SUPPLEMENTARY FIGURE 1

NH_4^+ increased MCs excitability in whole-cell current-clamp mode. (A) A recording of spontaneous firings in whole-cell current-clamp mode. (B,C) Pooled data showing the time course of resting membrane potential (RMP) and spike frequency during the 6-min application of NH_4Cl . Error bars represent standard error; * $p < 0.05$, ** $p < 0.01$, *** $p < 0.001$; one-way ANOVA with LSD *post hoc* test.

SUPPLEMENTARY FIGURE 2

NH_4^+ regulated MCs intrinsic excitability transiently. (A) Spontaneous firings in the presence of APV + NBQX + Bic + Stry (Ctrl, 1 min) and NH_4Cl + APV + NBQX + Bic + Stry (NH_4Cl , 8 min) in cell-attached mode. (B) Spontaneous firings during 0, 2, 4 and 6 min NH_4Cl application. (C–E) Scatter plots showing the amplitudes of inward current (I_{inward}), outward current (I_{outward}) and the ratio of I_{inward} to I_{outward} in spontaneous action potentials during the time course of NH_4Cl application. (F) Mean frequency during the time course of NH_4Cl application. (G) Whole-cell current-clamp recording of spontaneous action potentials with the injection current of 0 pA in the presence of APV + NBQX + Bic + Stry (Ctrl) and NH_4Cl + APV + NBQX + Bic + Stry (NH_4Cl). (H) Statistical curve showing the time course of RMP during the application of NH_4Cl . (I) The representative recording when injecting 10 pA current in current-clamp at a membrane potential of -60 mV before (Ctrl) and after NH_4Cl in the presence of APV + NBQX + Bic + Stry. (J) Histogram showing R_m before (Ctrl) and after NH_4Cl treatment from I, calculated using the function of $\tau = R_m C_m$, where τ is the time constant and C_m is the membrane capacitance. Error bars represent standard error; * $p < 0.05$, ** $p < 0.01$, *** $p < 0.001$; ns, not significant; one-way ANOVA with LSD *post hoc* test, paired Student's *t*-test.

SUPPLEMENTARY FIGURE 3

NH_4^+ -induced changes of voltage-gated sodium and potassium currents. (A) Raw electrophysiological traces showing inward currents (Na^+ current, I_{Na}) and outward currents (K^+ current, I_{K}) in Ctrl, 4-min and 8-min NH_4Cl . The protocol was performed by injecting step voltages from -70 mV to 40 mV with the increment of 10 mV at the holding potential of -70 mV in the presence of a cocktail of postsynaptic receptors blockers. Right panel representing the expanded I_{Na} in left panel. (B,C) Voltage-current relationship of I_{Na} and I_{K} in Ctrl, 4-min and 8-min NH_4Cl . (D) The number of activated I_{Na} events when injecting the voltage of -40 mV in Ctrl, 4-min and 8-min NH_4Cl . Error bars represent standard error; * $p < 0.05$, *** $p < 0.001$; one-way ANOVA with LSD *post hoc* test.

References

- Allert, N., Koller, H., and Siebler, M. (1998). Ammonia-induced depolarization of cultured rat cortical astrocytes. *Brain Res.* 782, 261–270. doi: 10.1016/s0006-8993(97)01288-2
- Aroniadou-Anderjaska, V., Ennis, M., and Shipley, M. T. (1999). Dendrodendritic recurrent excitation in mitral cells of the rat olfactory bulb. *J. Neurophysiol.* 82, 489–494. doi: 10.1152/jn.1999.82.1.489
- Back, A., Tupper, K. Y., Bai, T., Chirandand, P., Goldenberg, F. D., Frank, J. L., et al. (2011). Ammonia-induced brain swelling and neurotoxicity in an organotypic slice model. *Neurol. Res.* 33, 1100–1108. doi: 10.1179/1743132811Y.0000000046
- Bean, B. P. (2007). The action potential in mammalian central neurons. *Nat. Rev. Neurosci.* 8, 451–465. doi: 10.1038/nrn2148
- Boyd, A. M., Sturgill, J. F., Poo, C., and Isaacson, J. S. (2012). Cortical feedback control of olfactory bulb circuits. *Neuron* 76, 1161–1174. doi: 10.1016/j.neuron.2012.10.020
- Burch, R. E., Sackin, D. A., Ursick, J. A., Jetton, M. M., and Sullivan, J. F. (1978). Decreased taste and smell acuity in cirrhosis. *Arch. Intern. Med.* 138, 743–746. doi: 10.1001/archinte.1978.03630290047017
- Butterworth, R. F. (1993). Portal-systemic encephalopathy: A disorder of neuron-astrocytic metabolic trafficking. *Dev. Neurosci.* 15, 313–319. doi: 10.1159/000111350
- Cabrera-Pastor, A., Arenas, Y. M., Taoro-Gonzalez, L., Montoliu, C., and Felipo, V. (2019). Chronic hyperammonemia alters extracellular glutamate, glutamine and GABA and membrane expression of their transporters in rat cerebellum. Modulation by extracellular cGMP. *Neuropharmacology* 161:107496. doi: 10.1016/j.neuropharm.2019.01.011
- Cabrera-Pastor, A., Balzano, T., Hernandez-Rabaza, V., Malaguarnera, M., Llansola, M., and Felipo, V. (2018). Increasing extracellular cGMP in cerebellum *in vivo* reduces neuroinflammation, GABAergic tone and motor in-coordination in hyperammonemic rats. *Brain Behav. Immun.* 69, 386–398. doi: 10.1016/j.bbi.2017.12.013
- Cabrera-Pastor, A., Hernandez-Rabaza, V., Taoro-Gonzalez, L., Balzano, T., Llansola, M., and Felipo, V. (2016). *In vivo* administration of extracellular cGMP normalizes TNF-alpha and membrane expression of AMPA receptors in hippocampus and spatial reference memory but not IL-1beta, NMDA receptors in membrane and working memory in hyperammonemic rats. *Brain Behav. Immun.* 57, 360–370. doi: 10.1016/j.bbi.2016.05.011
- Calvert, J. W., Gundewar, S., Yamakuchi, M., Park, P. C., Baldwin, W. M. III, Lefer, D. J., et al. (2007). Inhibition of N-ethylmaleimide-sensitive factor protects against myocardial ischemia/reperfusion injury. *Circ. Res.* 101, 1247–1254. doi: 10.1161/CIRCRESAHA.107.162610
- Carlson, G. C., Shipley, M. T., and Keller, A. (2000). Long-lasting depolarizations in mitral cells of the rat olfactory bulb. *J. Neurosci.* 20, 2011–2021. doi: 10.1523/JNEUROSCI.20-05-02011.2000
- Catterall, W. A., Goldin, A. L., and Waxman, S. G. (2005). International union of pharmacology. XLVII. Nomenclature and structure-function relationships of voltage-gated sodium channels. *Pharmacol. Rev.* 57, 397–409. doi: 10.1124/pr.57.4.4
- Cauli, O., Rodrigo, R., Llansola, M., Montoliu, C., Monfort, P., Piedrafita, B., et al. (2009). Glutamatergic and gabaergic neurotransmission and neuronal circuits in hepatic encephalopathy. *Metab. Brain Dis.* 24, 69–80. doi: 10.1007/s11011-008-9115-4
- Chen, W. R., Midtgaard, J., and Shepherd, G. M. (1997). Forward and backward propagation of dendritic impulses and their synaptic control in mitral cells. *Science* 278, 463–467. doi: 10.1126/science.278.5337.463
- Chen, X. J., Zhou, H. Q., Ye, H. B., Li, C. Y., and Zhang, W. T. (2016). The effect of bilirubin on the excitability of mitral cells in the olfactory bulb of the rat. *Sci. Rep.* 6:32872. doi: 10.1038/srep32872
- De Saint Jan, D., Hirnet, D., Westbrook, G. L., and Charpak, S. (2009). External tufted cells drive the output of olfactory bulb glomeruli. *J. Neurosci.* 29, 2043–2052. doi: 10.1523/JNEUROSCI.5317-08.2009
- Deems, R. O., Friedman, M. I., Friedman, L. S., Munoz, S. J., and Maddrey, W. C. (1993). Chemosensory function, food preferences and appetite in human liver disease. *Appetite* 20, 209–216. doi: 10.1006/appe.1993.1021
- Gire, D. H., and Schoppa, N. E. (2009). Control of on/off glomerular signaling by a local GABAergic microcircuit in the olfactory bulb. *J. Neurosci.* 29, 13454–13464. doi: 10.1523/JNEUROSCI.2368-09.2009
- Gire, D. H., Franks, K. M., Zak, J. D., Tanaka, K. F., Whitesell, J. D., Mulligan, A. A., et al. (2012). Mitral cells in the olfactory bulb are mainly excited through a multistep signaling path. *J. Neurosci.* 32, 2964–2975. doi: 10.1523/JNEUROSCI.5580-11.2012
- Hayar, A., Karnup, S., Shipley, M. T., and Ennis, M. (2004). Olfactory bulb glomeruli: External tufted cells intrinsically burst at theta frequency and are entrained by patterned olfactory input. *J. Neurosci.* 24, 1190–1199. doi: 10.1523/JNEUROSCI.4714-03.2004
- Heiser, C., Haller, B., Sohn, M., Hofauer, B., Knopf, A., Mühlhng, T., et al. (2018). Olfactory function is affected in patients with cirrhosis depending on the severity of hepatic encephalopathy. *Ann. Hepatol.* 17, 822–829. doi: 10.5604/01.3001.0012.3143
- Hernandez-Rabaza, V., Cabrera-Pastor, A., Taoro-Gonzalez, L., Malaguarnera, M., Agusti, A., Llansola, M., et al. (2016). Hyperammonemia induces glial activation, neuroinflammation and alters neurotransmitter receptors in hippocampus, impairing spatial learning: Reversal by sulforaphane. *J. Neuroinflammation* 13:41. doi: 10.1186/s12974-016-0505-y
- Isaacson, J. S., and Strowbridge, B. W. (1998). Olfactory reciprocal synapses: Dendritic signaling in the CNS. *Neuron* 20, 749–761. doi: 10.1016/s0896-6273(00)81013-2
- Izumi, Y., Svrakic, N., O'Dell, K., and Zorumski, C. F. (2013). Ammonia inhibits long-term potentiation *via* neurosteroid synthesis in hippocampal pyramidal neurons. *Neuroscience* 233, 166–173. doi: 10.1016/j.neuroscience.2012.12.035
- Jayakumar, A. R., and Norenberg, M. D. (2018). Hyperammonemia in hepatic encephalopathy. *J. Clin. Exp. Hepatol.* 8, 272–280. doi: 10.1016/j.jceh.2018.06.007
- Kosenkov, A. M., Gaidin, S. G., Sergeev, A. I., Teplov, I. Y., and Zinchenko, V. P. (2018). Fast changes of NMDA and AMPA receptor activity under acute hyperammonemia *in vitro*. *Neurosci. Lett.* 686, 80–86. doi: 10.1016/j.neulet.2018.08.054
- Landis, B. N., Konnerth, C. G., and Hummel, T. (2004). A study on the frequency of olfactory dysfunction. *Laryngoscope* 114, 1764–1769. doi: 10.1097/00005537-200410000-00017
- Lazarenko, R. M., DelBove, C. E., Strothman, C. E., and Zhang, Q. (2017). Ammonium chloride alters neuronal excitability and synaptic vesicle release. *Sci. Rep.* 7:5061. doi: 10.1038/s41598-017-05338-5
- Llansola, M., Sanchez-Perez, A., Cauli, O., and Felipo, V. (2005). Modulation of NMDA receptors in the cerebellum. 1. Properties of the NMDA receptor that modulate its function. *Cerebellum* 4, 154–161. doi: 10.1080/14734220510007996
- Lu, B., Su, Y., Das, S., Liu, J., Xia, J., and Ren, D. (2007). The neuronal channel NALCN contributes resting sodium permeability and is required for normal respiratory rhythm. *Cell* 129, 371–383. doi: 10.1016/j.cell.2007.02.041
- Margrie, T. W., Sakmann, B., and Urban, N. N. (2001). Action potential propagation in mitral cell lateral dendrites is decremental and controls recurrent and lateral inhibition in the mammalian olfactory bulb. *Proc. Natl. Acad. Sci. U.S.A.* 98, 319–324. doi: 10.1073/pnas.98.1.319
- Montes-Cortes, D. H., Olivares-Corichi, I. M., Rosas-Barrientos, J. V., Manuel-Apolinar, L., Martinez-Godinez, M. L. A., Hernández-López, J. C., et al. (2020). Characterization of oxidative stress and ammonia according to the different grades of hepatic encephalopathy. *Dig. Dis.* 38, 240–250. doi: 10.1159/000503097
- Moran, A. K., Eiting, T. P., and Wachowiak, M. (2021). Dynamics of glutamatergic drive underlie diverse responses of olfactory bulb outputs *in vivo*. *eNeuro* 8. doi: 10.1523/ENEURO.0110-21.2021
- Nagayama, S., Homma, R., and Imamura, F. (2014). Neuronal organization of olfactory bulb circuits. *Front. Neural Circuits* 8:98. doi: 10.3389/fncir.2014.0098
- Nicoll, R. A., and Jahr, C. E. (1982). Self-excitation of olfactory bulb neurones. *Nature* 296, 441–444. doi: 10.1038/296441a0
- Oja, S. S., Saransaari, P., and Korpi, E. R. (2017). Neurotoxicity of ammonia. *Neurochem. Res.* 42, 713–720. doi: 10.1007/s11064-016-2014-x
- Ong, J. P., Aggarwal, A., Krieger, D., Easley, K. A., Karafa, M. T., Van Lente, F., et al. (2003). Correlation between ammonia levels and the severity of hepatic encephalopathy. *Am. J. Med.* 114, 188–193. doi: 10.1016/s0002-9343(02)01477-8
- Padmanabhan, K., and Urban, N. N. (2010). Intrinsic biophysical diversity decorrelates neuronal firing while increasing information content. *Nat. Neurosci.* 13, 1276–1282. doi: 10.1038/nn.2630

- Pidoplichko, V. I., and Dani, J. A. (2006). Acid-sensitive ionic channels in midbrain dopamine neurons are sensitive to ammonium, which may contribute to hyperammonemia damage. *Proc. Natl. Acad. Sci. U.S.A.* 103, 11376–11380. doi: 10.1073/pnas.0600768103
- Rangroo Thrane, V., Thrane, A. S., Wang, F., Cotrina, M. L., Smith, N. A., Chen, M., et al. (2013). Ammonia triggers neuronal disinhibition and seizures by impairing astrocyte potassium buffering. *Nat. Med.* 19, 1643–1648. doi: 10.1038/nm.3400
- Rao, V. L., Agrawal, A. K., and Murthy, C. R. (1991). Ammonia-induced alterations in glutamate and muscimol binding to cerebellar synaptic membranes. *Neurosci. Lett.* 130, 251–254. doi: 10.1016/0304-3940(91)90408-1
- Sanchez-Perez, A. M., and Felipo, V. (2006). Chronic exposure to ammonia alters basal and NMDA-induced phosphorylation of NMDA receptor-subunit NR1. *Neuroscience* 140, 1239–1244. doi: 10.1016/j.neuroscience.2006.03.004
- Sancho-Alonso, M., Taoro-Gonzalez, L., Cabrera-Pastor, A., Felipo, V., and Teruel-Marti, V. (2022). Hyperammonemia alters the function of AMPA and NMDA receptors in hippocampus: Extracellular cGMP reverses some of these alterations. *Neurochem. Res.* 47, 2016–2031. doi: 10.1007/s11064-022-03588-y
- Schoppa, N. E., and Westbrook, G. L. (2001). NMDA receptors turn to another channel for inhibition. *Neuron* 31, 877–879. doi: 10.1016/s0896-6273(01)00442-1
- Szerb, J. C., and Butterworth, R. F. (1992). Effect of ammonium ions on synaptic transmission in the mammalian central nervous system. *Prog. Neurobiol.* 39, 135–153. doi: 10.1016/0301-0082(92)90008-3
- Temmel, A. F., Pabinger, S., Quint, C., Munda, P., Ferenci, P., and Hummel, T. (2005). Dysfunction of the liver affects the sense of smell. *Wien. Klin. Wochenschr.* 117, 26–30. doi: 10.1007/s00508-004-0303-x
- Wang, J. W., Wong, A. M., Flores, J., Vossahl, L. B., and Axel, R. (2003). Two-photon calcium imaging reveals an odor-evoked map of activity in the fly brain. *Cell* 112, 271–282. doi: 10.1016/s0092-8674(03)00004-7
- Yonden, Z., Aydin, M., Kilbas, A., Demirin, H., Sutcu, R., and Delibas, N. (2010). Effects of ammonia and allopurinol on rat hippocampal NMDA receptors. *Cell Biochem. Funct.* 28, 159–163. doi: 10.1002/cbf.1636
- Zucco, G. M., Amodio, P., and Gatta, A. (2006). Olfactory deficits in patients affected by minimal hepatic encephalopathy: A pilot study. *Chem. Senses* 31, 273–278. doi: 10.1093/chemse/bjj029